



Facile Synthesis of Silver Nanoparticles Using *Lantana trifolia* Aqueous Extracts and Their Antibacterial Activity

Edwin Shigwenya Madivoli¹ · Patrick Gachoki Kareru¹ · Anthony Ngure Gachanja¹ · Samuel Mutuura Mugo² · David Sujee Makhanu³ · Sammy Indire Wanakai¹ · Yahaya Gavamukulya⁴

Received: 28 November 2019 / Accepted: 26 December 2019
© Springer Science+Business Media, LLC, part of Springer Nature 2020

Abstract

Synthesis of metallic nanoparticles using secondary metabolites present in plant extracts has attracted attention. In this study, *Lantana trifolia* aqueous extracts were used to synthesize silver nanoparticles (AgNPs) which were then screened for their antimicrobial activity. The morphology, size and functional groups present in AgNPs was evaluated using electron microscopy and Fourier transform infrared spectroscopy (FT-IR). The role of temperature, reaction time and concentration of precursor ion were evaluated by measuring the surface plasmon resonance of AgNPs using UV–Vis spectroscopy. The crystal structure, hydrodynamic diameters and redox potential were evaluated using powder X-ray diffractometer (PXRD), dynamic light scattering (DLS) and cyclic voltammetry respectively. The data obtained in this study revealed that increase in the reaction time led to an increase in surface plasmon resonance of AgNPs while the increase in temperature from 20 to 35 °C increased the rate of AgNPs synthesis. The XRD diffractogram revealed that the particles were composed of silver with $2\theta = 38.36, 44.428, 54.89, \text{ and } 57.87$, corresponding to the silver crystal planes of (111), (200), (220), and (311). The diameters of the nanoparticles were between 35 and 70 nm, and they had moderate antimicrobial activity against *E. coli*, *P. aeruginosa*, *C. albicans*, *S. aureus* and *B. subtilis*.

Keywords Silver nanoparticles · Morphology · Antimicrobial activity

1 Introduction

Bacterial resistance is a major public health concern because of its negative impact on the health care system as existing antibiotics lose efficacy [1]. Metallic nanoparticles effect

antimicrobial activity through membrane protein damage, super peroxide radicals or generation of ions that can interfere with cell granules. These particles have the potential to inhibit formation of advanced glycation end products and they can be used as anticancer therapies [2, 3]. Moreover, metallic nanoparticles such as silver nanoparticles (AgNPs) have been reported to alter the metabolic activity of bacteria and preventing biofilm formation [4]. The antibacterial characteristics of AgNPs are influenced by their size, shape, concentration and colloidal state. With respect to size, smaller nanoparticles have a large surface area in contact with the bacterial cells and they can reach the cytoplasm of the cell as compared to larger nanoparticles. Hence, for enhanced antibacterial activity, the size of the nanoparticles should be less than 50 nm but for the case of silver it has been reported that they have increased stability, biocompatibility and enhanced antimicrobial activity if their size is between 10 and 15 nm [5]. The AgNPs can be synthesized through electrochemical or photochemical reduction and by controlled chemical reduction of Ag ions in solution. These wet-chemical methods involve reduction of Ag ions in solution

Electronic supplementary material The online version of this article (<https://doi.org/10.1007/s10904-019-01432-5>) contains supplementary material, which is available to authorized users.

✉ Edwin Shigwenya Madivoli
edwinshigwenya@gmail.com

¹ Department of Chemistry, Jomo Kenyatta University of Agriculture and Technology, P.O Box 62, Nairobi 000-00200, Kenya

² Chemistry Department, McEwan University, 10700-104 Avenue, Edmonton, AB T5J 4S2, Canada

³ Department of Physical & Biological Sciences, Karatina University, P.O Box 1957-10101, Karatina, Kenya

⁴ Department of Biochemistry and Molecular Biology, Faculty of Health Sciences, Busitema University, P.O Box 1460, Mbale, Uganda

to metallic AgNPs with parameters such as the choice of reducing agents, the concentration of reagents, temperature, pH, mixing rate and reaction time manipulated to control the size, shape and rate at which they are formed [6]. When compared to wet chemical methods, the use of plant extracts to synthesize metallic nanoparticles is desirable as it is faster, environmentally friendly and employs the use of mild reaction conditions [7]. Green synthesized AgNPs are not only biocompatible but the method is cost-effective as it provides the possibility of supporting larger synthesis and the reduction occurs in 2–4 h and through manipulation of reaction conditions such as pH, substrate concentration, temperature and the reaction time the size of the nanoparticles can be controlled [8]. With increased antimicrobial properties, AgNPs are currently used in consumer and industrial applications such as food packaging [9], coatings on medical devices [10, 11], water disinfectants, antimicrobial textile fabrics [12, 13] and cosmetic products [14].

In this study, AgNPs were synthesized using aqueous extracts of *Lantana trifolia* which has been reported to contain a variety of secondary metabolites such as flavonoids, tannins, chalcones, coumarins and phenolic acids which can serve as reducing and capping agents [15]. The nanoparticles were then characterized using Fourier-transform infrared spectrophotometer (FTIR) to determine the functional groups present while the crystalline phase was determined using wide-angle X-ray diffractometer. The surface morphology and size of the nanoparticles were evaluated using a scanning electron microscope (SEM), dynamic light scattering (DLS) and a Transmission electron microscope (TEM) respectively. The antimicrobial properties and antioxidant potential of the synthesized nanoparticles were evaluated using disc diffusion assay and cyclic voltammetry.

2 Materials and Methods

2.1 Extraction of Secondary Metabolites

Fresh leaves of *Lantana trifolia* were collected from Thika Sub-County, Kiambu County in Kenya, washed with distilled water and air-dried at room temperature before pulverization using a milling machine (locally assembled no model number). Aqueous extracts were obtained by extraction of 100 mg of ground sample in 500 ml of water in a Soxhlet apparatus.

2.2 Synthesis of AgNPs using *L. trifolia* Extracts

In the synthesis of AgNPs, the effects of temperature, concentration of AgNO₃ solution and reaction time extracts were investigated to ascertain their role during the reaction process. In 3 mL aqueous solution of AgNO₃ solution (0.5,

1, 1.5 mM), 1 mL of the plant extracts was added into the solution and the formation of AgNPs monitored using a Shimadzu UV–Vis 1800 spectrophotometer in the range of 300–800 nm [16]. The role of temperature during synthesis was evaluated by adding 200 µL of 0.1 M AgNO₃ solution to 2.5 mL aqueous extracts and the reaction carried out at 20, 25, 30 and 35 °C for 2 h respectively. The rate of AgNPs formation was calculated from the absorbance value (λ_{\max}) that was observed after 3 h by plotting a graph of $\ln A/A_0$ against time while the rate of formation (k) was obtained from the slope of the curves [17]. The particles obtained were washed with distilled water and ethanol to remove impurities and dried before further analysis.

2.3 Characterization of AgNPs

The functional groups present were determined by a Shimadzu Fourier Transform Infrared spectrophotometer, Model FTS- 8000 (Shimadzu Corporation, Japan). The KBr pellets were prepared by grinding 10 mg of samples, with 250 mg KBr (FT-IR grade). The 13 mm KBr pellets were prepared in a standard device under a pressure of 75 kN cm⁻² for 3 min. The spectral resolution was set at 4 cm⁻¹ and the scanning range from 400 to 4000 cm⁻¹ [18, 19]. The spectral resolution was set at 4 cm⁻¹ and the scanning range from 400 to 4000 cm⁻¹ [18, 19]. The powder XRD profile of the AgNPs was examined using a STOE STADIP P X-ray Powder Diffraction System (STOE and Cie GmbH, Darmstadt, Germany). The X-ray generator was equipped with a copper tube operating at 40 kV and 40 mA and irradiating the sample with a monochromatic CuK α radiation with a wavelength of 0.1545 nm. XRD spectra was acquired at room temperature over the 2 θ range of 2°–90° at 0.05° intervals with a measurement time of 1 s per 2 θ intervals [20]. The thermal properties of AgNPs was evaluated using a Mettler Toledo Thermal Gravimetric DSC/TGA 3 + system (Mettler-Toledo GmbH, Switzerland). 10 mg of the sample was heated from 25 to 500 °C at 10 °C/min cooled to 25 °C [18, 21]. The particle size distribution, zeta potential and poly-dispersibility index of the FeNPs solution were measured using a Bechman Coulter DelsaMax pro dynamic light scattering analyzer (Indianapolis, United States). The morphology of AgNPs was evaluated using a scanning electron microscope FEI XL30 Sirion FEG (Oxford Instruments Plc, Abingdon, United Kingdom) operated at an accelerating voltage of 30 kV. The system was equipped with an energy dispersive x-ray spectrometer (EDS) system from EDAX having a lithium doped silicon detector (Wang et al. [22]). TEM micrographs were acquired on a Tecnai G2 Spirit (Thermo Fisher Scientific, Oregon USA) operated at 120 kV after suspending the pulp fibers in ultrapure water (18 M Ω cm Barnstead Genpure UV-TOC, Thermo Fisher scientific, Germany), and drop casting on carbon films 300 mesh (Electron

microscopy science, CF300-CU). The particle size distribution, zeta potential and poly-dispersibility index was measured using a Bechman Coulter DelsaMax pro Dynamic light scattering analyzer (Indianapolis, United States).

2.4 Disc Diffusion Assay

The antibacterial activity of AgNPs against the selected Gram-negative, gram positive and fungal pathogens was carried out using Kirby–Bauer disk diffusion susceptibility test. The bacteria strains were then spread on the Mueller–Hinton agar (MHA) (Merck, Germany) using a sterile cotton swab. Sterile blank antimicrobial susceptibility disk was used in the test. The disks were loaded with *L. trifolia* leaves extracts and a solution containing green synthesized AgNPs separately, placed on the agar plate and incubated at 37 °C for 24 h [23].

3 Results and Discussions

3.1 UV–VIS Analysis of AgNPs

Figure 1 illustrates the time dependence of the AgNPs formation using *L. trifolia* extracts as determined by UV/Vis spectroscopy.

Silver nanoparticles exhibit surface plasmon resonance (SPR) which allows the absorption and scattering of incident radiation that can be measured using a UV–Vis spectrophotometer. The SPR band intensity and wavelength is dependent on particle properties such as the shape, structure, metal type, size, and the dielectric material surrounding the medium [24]. In order to understand the impact of time, temperature and the concentration of Ag^+ ion during synthesis, the reactions were carried out under different temperatures, concentration of Ag^+ ions and time. As observed in Fig. 1,

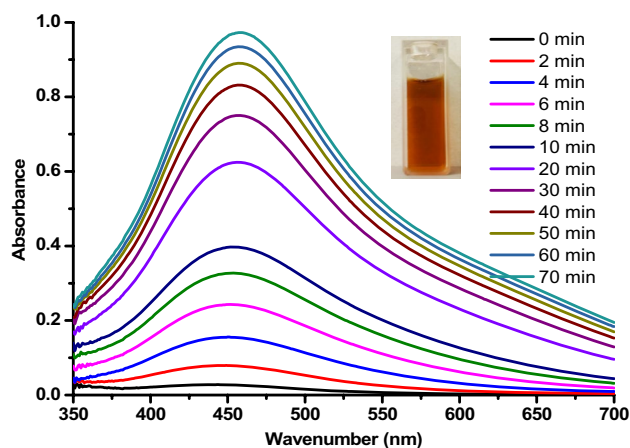


Fig. 1 Measurement of absorbance against time

the absorption spectrum of AgNPs spanned a wide range from 330 to 600 nm with the surface plasmon resonance (SPR) peak, an indicator for AgNPs formation, centred at 443 nm [25, 26]. Increasing the amount of extract used and the reaction time resulted to a subsequent increase in the amount of AgNPs formed in solution as a result, the surface plasmon peak increased. However, the observed increase in SPR was stable after 2 h of incubation, which indicated that the synthesis was complete. The SPR spectra of AgNPs synthesized using 0.5 mM AgNO_3 solution showed a sharper and stronger absorption band as compared higher concentration (1 mM and 1.5 mM), which were less intense (Fig. 3) [26]. Moreover, presence of a broad plasmon band that extends from 360 to 550 nm with an absorption tail at higher wavelength (Fig. 1, 2, 3) could be due to the

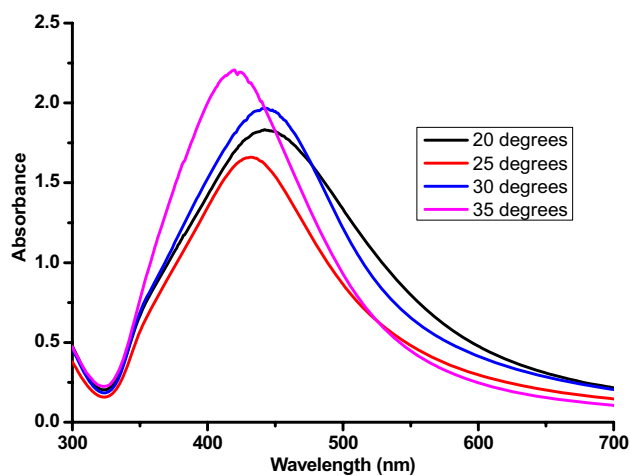


Fig. 2 Effect of temperature on the size of AgNPs synthesized using *L. trifolii* extracts after 2 h

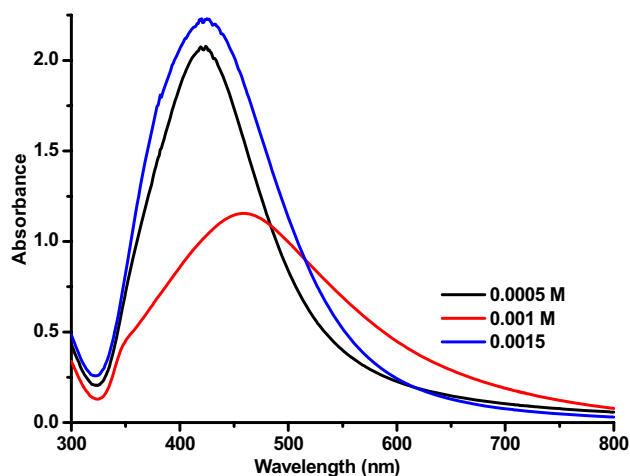


Fig. 3 Variation of ratio of extracts volume to concentration of Ag used after 2 h

multi-size distribution of the nanoparticles [17]. The findings in this study are in agreement with observations made in literature since a bathochromic shift in the UV–Vis spectra was observed when the temperature of the reaction media was decreased from 35 to 20 °C [27]. However, a decrease in the reaction temperature led to a broad band being observed, which is associated with the presence of larger particles. At lower temperatures, the nanoparticles aggregated hence the broad UV spectra observed at 20 °C as compared to higher temperature (35 °C), in which an increase in the optical density and the SPR was as a result of an increase in the number of synthesized particles. The red-shift observed was due to the delocalization and sharing of conduction electrons near each particle surface among neighboring particles [28]. Broadening and bathochromic shift are associated with agglomeration or increase in particle sizes, which increase the scattering of the solution [26]. The energy band gap can be estimated from tauc plot between $(\alpha h\nu)^2$ versus energy of photon ($h\nu$). The intercept of the tangent on the tauc plot give a direct band gap for $n = 1$. The band gap energy for AgNPs synthesized at 30 °C was determined from Tauc plot (Fig. 4) and it was found to be 2.36 eV.

3.2 FT-IR spectra of AgNPs

The FT-IR spectra of AgNPs synthesized using *L. trifolia* extracts are depicted in Fig. 5.

From the IR spectra (Fig. 5), the vibration frequencies observed at 3361, 2918, 1379 and 1257 cm^{-1} are typically reported to be vibrational frequencies due to presence of OH stretching, C–H stretching, OH bending (phenolic compounds) and C–N stretching of amines or C–O aromatic. These functional groups are typically present in phenolic compounds such as flavanoids, phenolic acids, in terpenes

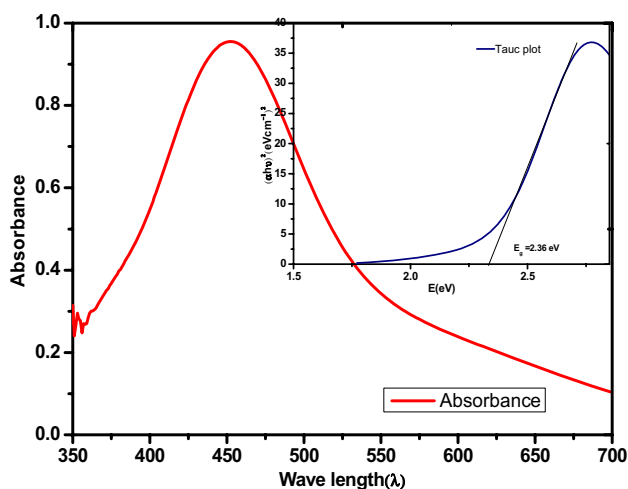


Fig. 4 UV–Vis spectrum of AgNPs synthesized at 30 °C. Inset Tauc plot for AgNPs

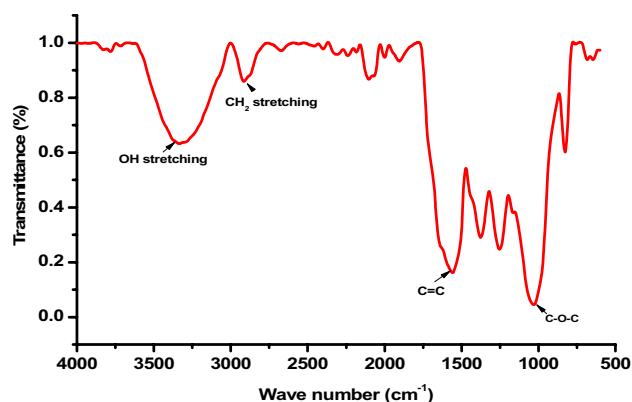


Fig. 5 FT-IR spectra of AgNPs synthesized using *L. trifolia* extracts

and terpenoids, and in nitrogen containing compounds such as alkaloids, amino acids and indoles [29]. The vibrational frequencies at 1039, 813, 753 and 683 cm^{-1} are typical of C–O stretching, C=C bending, C–H bending and C=C bending respectively [30]. It is worth noting that the position of the bands due to the C=C stretching vibration and the CH_2 in-plane deformation vibration are influenced by presence of a metal- π bond coordination system. Coordination of an organic molecule to a metal atom through π -bonding reduces the C=C stretching frequency and brings it closer to the CH_2 deformation frequency which allows increased coupling to occur. As a result, coordination of Ag to an organic molecule decreases the C=C stretching frequency which means that the band due to C=C vibration occurs at 1596 cm^{-1} rather than at around 1620 cm^{-1} [30].

3.3 X-ray Diffractogram of Silver Nanoparticles

The X-ray diffractogram of the synthesized AgNPs are depicted in Fig. 6.

From Fig. 6, wide angle X-ray diffraction analysis confirmed the crystalline nature of mediated AgNPs based on the diffraction peaks centred at $2\theta = 38, 44, 55,$ and 58 , corresponding to the silver crystal planes of (111), (200), (220), and (311), respectively. However, the peaks at $2\theta = 28, 33, 47$ correspond to AgCl planes (111), (200) and (202) which can be attributed to the presence of chloride ion in the aqueous extracts which lead to formation of AgCl together Ag^0 [17]. It is worth noting that pristine silver nanoparticles are not chemically stable in the environment and they strongly react with inorganic ligands such as sulphide and chloride once the silver is oxidized. Being one of the most prevalent monovalent anions in the natural aqueous systems, chloride ions are present in plant extracts used during synthesis of AgNPs [31]. As such during synthesis of AgNPs using plant extracts, the interaction between Cl^- and Ag^+ leads to

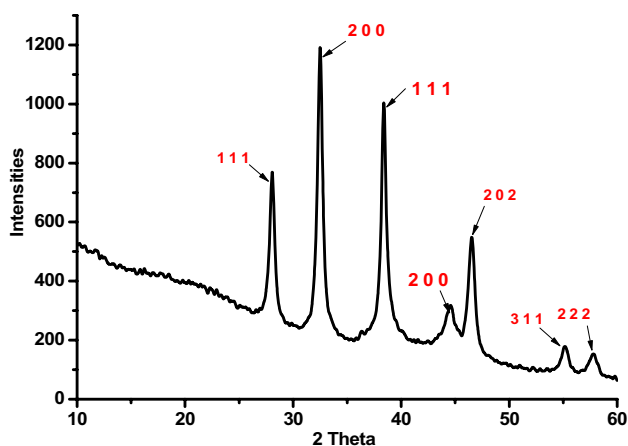


Fig. 6 X-ray diffractogram of biosynthesized AgNPs

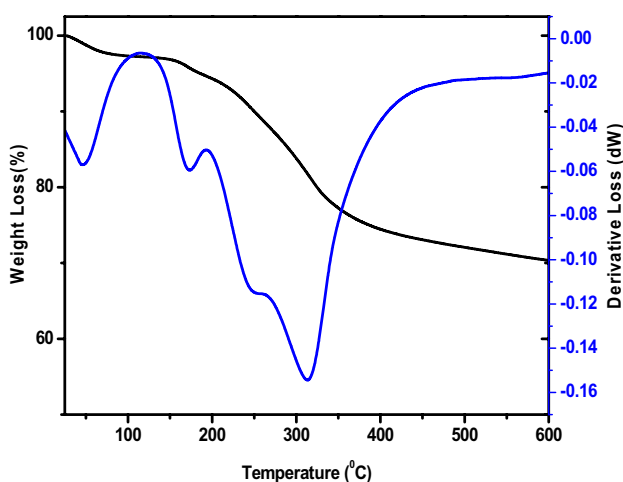


Fig. 7 TGA and DTGA of AgNPs synthesized using *L. trifolia* extracts

formation of both AgCl and AgNPs hence their presence in the XRD profile.

3.4 TGA-DTGA Thermograms of AgNPs

The thermal properties of AgNPs synthesized using *L. trifolia* are depicted in Fig. 7.

The TGA thermograms of AgNPs synthesized using *L. trifolia* had three distinct degradation phases at 47, 172, and 251 °C with maximum degradation occurring at 313 °C. These degradation stages were followed by subsequent changes in mass of the sample with a final mass loss of 28.9% being observed. The decomposition occurring at 173 °C can be associated with the removal of the organic layer surrounding the nanoparticles, which can also be linked to the high ash content [8].

3.5 SEM Micrographs of AgNPs

The morphology of AgNPs synthesized using *L. trifolia* are depicted in Fig. 8.

From SEM micrograph obtained (Fig. 8), the particle appeared to be amorphous in nature. While green synthesis of metallic nanoparticle has in the recent past obtained much attention due to their environmental friendliness, one major drawback of this approach is that the nanoparticles are usually amorphous in nature [8]. This is due to the presence of a secondary metabolite coating that surrounds the nanoparticles and prevents their reaction with species such OH⁻ present in the reaction media thereby preventing formation of metallic oxides. The organic coating surrounding AgNPs can also be accounted for since from the FT-IR spectra (Fig. 2) in which presence of functional groups associated with secondary metabolites were observed [7, 8].

3.6 Size Distribution Measurements

The diameter of silver nanoparticles synthesized using *L. trifolia* was measured using dynamic light scattering and the results are depicted in Fig. 9, Table 1.

The results show that the average size of particle synthesized using different temperatures was in the range between 35 and 65 nm in diameter. DLS measures the hydrodynamic diameter, which is the diameter of the particle plus ions or molecules that are attached to the surface and moves with the AgNPs in solution. It was observed that variation in temperature played a role in the size of the synthesized nanoparticles, which is in agreement with observations made under UV-Vis analysis [8]. From Fig. 10, the effect of temperature on the size of the synthesized nanoparticles could be clearly observed as at higher and lower temperatures, the diameter of the nanoparticles was found to be 60 ± 3 , 37.0 ± 0.7 , 46 ± 1.0 and 48 ± 3 for 35, 30, 25, and 20 °C respectively.

3.7 TEM Micrographs of AgNPs

TEM micrographs and size distribution of green synthesized AgNPs are depicted in Fig. 10.

From Fig. 10, it can be observed that AgNPs were spherical in nature. Measurement of size of the AgNPs revealed that under optimal reaction conditions, the particles were spherical with variable sizes between 5 and 70 nm in diameter. The results obtained from TEM analysis were in agreement with dynamic light scattering since from DLS measurements the particles were found to be polydisperse. This variability in particle size has been associated with the inability of the secondary metabolites to control particle size during growth as compared to other methods that employ the using of polymeric materials to control the size of the nanoparticles during synthesis [27].

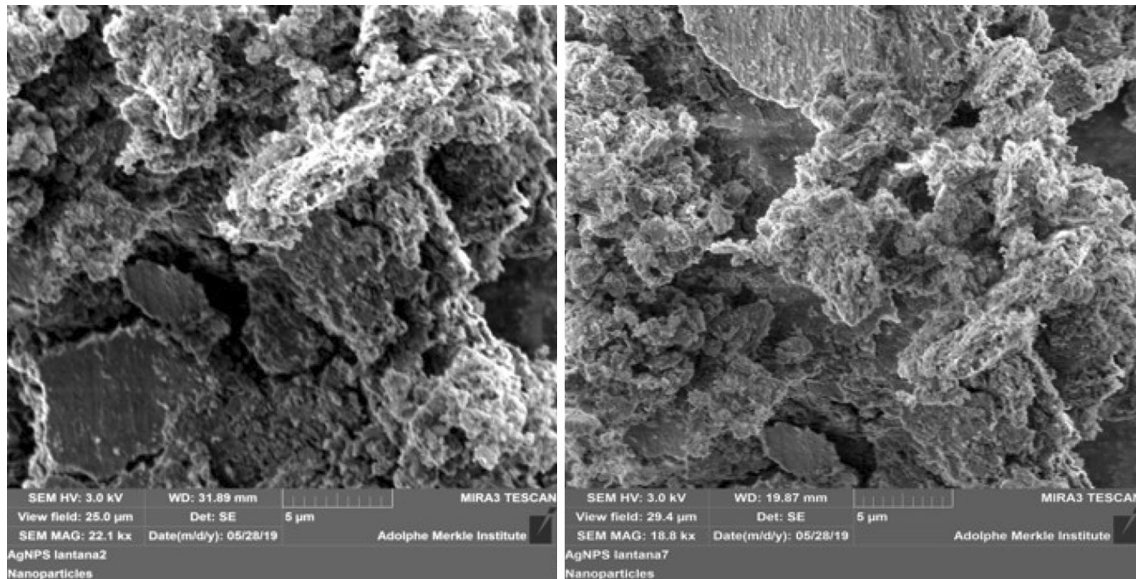


Fig. 8 SEM micrographs of green synthesized AgNPs

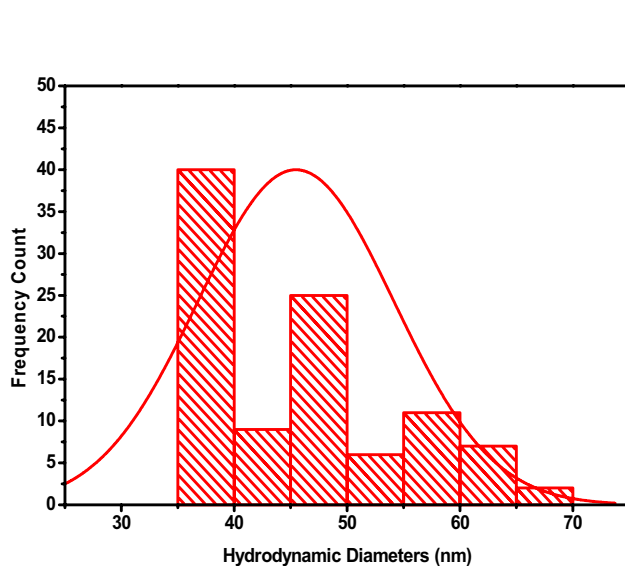


Fig. 9 Hydrodynamic diameter distribution of AgNPs synthesized at various temperatures

Table 1 Hydrodynamic diameter, Zeta potential and Poly-dispersibility index (PDI) of AgNPs

Sample	Hydrodynamic diameters	Zeta potential (mV)	PDI
T35	60 ± 3	-22 ± 4	0.57 ± 0
T30	37 ± 1	-6 ± 1	0.56 ± 0
T25	46 ± 1	-22 ± 1	0.57 ± 0
T20	48 ± 3	-18 ± 4	0.57 ± 0

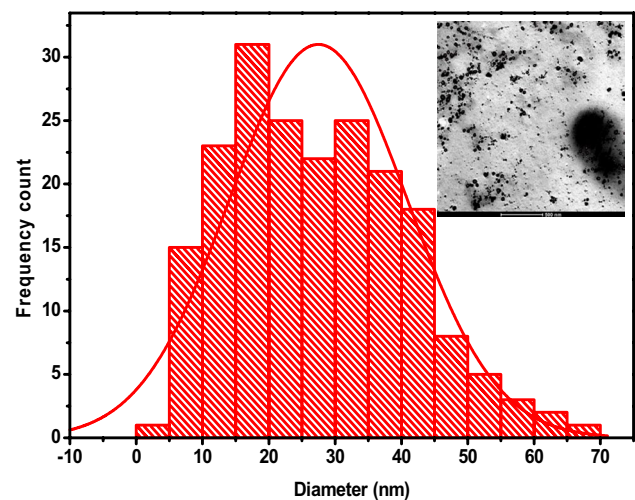


Fig. 10 Particle Diameter distribution of AgNPs synthesized using *L. trifolia* extracts

3.8 Cyclic Voltammetry

The redox potential of green synthesized AgNPs was evaluated using cyclic voltammetry and the results are depicted in Fig. 11.

The total reducing power is defined as the ability of certain molecules to act as electron donors or protons receptors in oxidation–reduction reactions. From the data obtained in CV (Fig. 11), it follows that the most important parameters are the peak potential and the peak current. The peak potential correlates with the type of reductant; low oxidation potentials are associated with a greater facility or strength

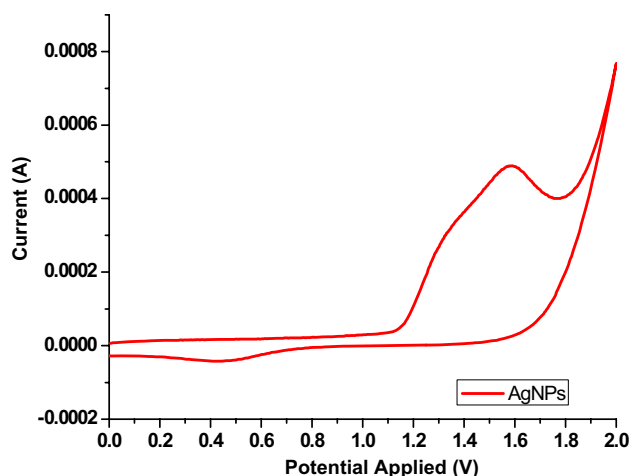


Fig. 11 Cyclic voltammogram of AgNPs synthesized using *L. trifolia* extracts

of a given molecule for the electron donation and, thus, to act as antioxidant; peak current is directly proportional to the antioxidant concentration according to Randles–Sevcik equation [32]. As can be observed, the cyclic voltammograms gave an anodic (positive) peak at 159 mV, which correspond to the total oxidation potential of AgNPs [33].

3.9 Antimicrobial Studies

The antimicrobial activity of the synthesized nanoparticles was evaluated against selected microorganisms and the results are depicted in Table 2.

From the results obtained, the synthesized AgNPs were more potent on gram positive bacteria *S. aureus* as compared to when compared to gram negative bacteria *E. coli* and *P. aeruginosa*, gram negative bacteria *B. subtilis* and the fungal strain *C. albicans*. The zones of inhibition were highest in *S. aureus* followed by *C. albicans*, *E. coli* and *P. aeruginosa* and lowest in *B. subtilis* (Table 3). It has been demonstrated that the antibacterial effect of AgNPs on gram negative bacteria is higher than on gram positive bacteria as a result of the thickness of cell wall. In gram positive bacteria, the cell wall thickness is 30 nm while in gram negative bacteria the cell wall thickness is between 3 and 4 nm and is mainly composed of peptidoglycan [5, 34]. Due to this difference, gram

Table 3 Inhibition zones for standard antibiotics

Antibiotic standards	SA	PA	BS	EC	CA
Minimum inhibition zones (Mean \pm SD) in mm					
SX	8.0 \pm 0.0	14.0 \pm 0.0	12.0 \pm 0.0	17.0 \pm 1.4	9.0 \pm 0.0
GEN	8.0 \pm 0.0	9.0 \pm 0.0	8.0 \pm 0.0	13.0 \pm 0.0	NI
AMC	9.0 \pm 0.0	NI	8.0 \pm 0.0	14.0 \pm 0.0	NI
NX	9 \pm 3	14.0 \pm 0.0	12.0 \pm 0.0	28.0 \pm 0.0	NI
CTR	32 \pm 1	9.0 \pm 0.0	NI	24.5 \pm 2.1	NI
NIT	NI	NI	8.0 \pm 0.0	12.0 \pm 0.0	NI
OF	NI	11.0 \pm 0.0	9. \pm 1	27.0 \pm 2.8	12.00 \pm 0.00
NA	NI	NI	9.0 \pm 0.0	15.0 \pm 2.8	NI

SX sulphamethoxazole (25 μ g); GEN gentamicin (10 μ g); AMC amoxycylav (20/10 μ g); NX norfloxacin (10 μ g); CTR ceftriaxone (30 μ g); NIT: nitrofurantoin (200 μ g); OF ofloxacin (10 μ g); NA nalidixic acid (30 μ g); NI no inhibition; PA *Pseudomonas aeruginosa*; BS *Bacillus subtilis*; EC *Escherichia coli*; CA *Candida albicans*; SA *Staphylococcus aureus*

negative bacteria are more susceptible to AgNPs which are able to anchor themselves on bacteria cell wall, infiltrate it and thereby damaging the cell membrane leading to cellular content leakage and bacterial death [34]. In our study, the AgNPs were more potent on gram negative bacteria *E. coli* and *P. aeruginosa* as compared to the gram-positive bacteria *B. subtilis*. However, when compared to the gram-positive bacteria *S. aureus*, AgNPs had higher potency to this strain of bacteria as compared to the gram-negative bacteria that were studied (Fig. 12).

4 Conclusion

Silver nanoparticles were synthesized using *lantana trifolia* extracts. Characterization of the synthesized nanoparticles revealed that the nanoparticles had variable sizes depending on reaction conditions and they contained crystalline indices reported for silver nanoparticles. Morphology of the nanoparticles as studied by scanning electron microscopy revealed that the particles were amorphous in nature while TEM micrographs and DLS data revealed that the particles were polydisperse with variable diameters.

Table 2 Antimicrobial activity of AgNPs against selected microorganisms

Concentration	Gram negative		Fungi <i>C. albicans</i>	Gram positive	
	<i>E. coli</i>	<i>P. aeruginosa</i>		<i>S. aureus</i>	<i>B. subtilis</i>
10 ³	11 \pm 1	11 \pm 1	12 \pm 1	16 \pm 1.7	8.7 \pm 0.6
10 ²	9 \pm 1	8.7 \pm 0.6	9.3 \pm 0.6	15 \pm 1	8 \pm 1
10 ¹	7.3 \pm 0.6	7.3 \pm 0.6	8 \pm 1	13.7 \pm 1.5	7.3 \pm 0.6
1	7 \pm 1	NI	7.3 \pm 0.6	9.7 \pm 1.2	NI

Fig. 12 Antimicrobial activity of AgNPs against selected microorganisms



Acknowledgements The authors would like to thank the Department of Chemistry, Jomo Kenyatta University of Agriculture and Technology and Sino Africa Joint Research Centre (SAJOREC) for provision of facilities where part of the work was done. The authors also acknowledge the financial support of the National research fund, AFRICA-ai-JAPAN Project JFY 2018/2019 and Research Production and Extension division, Jomo Kenyatta University of Agriculture and Technology (JKUAT-RPE) for their financial support. The authors also acknowledge the financial support of the Federal Commission of Scholarships for a one-year PhD research stay at the University of Fribourg under Prof. Katharina M. Fromm.

Compliance with Ethical Standards

Conflict of interest All authors declare that they have no conflict of interest.

References

1. D. van Duin, D.L. Paterson, Multidrug-resistant bacteria in the community trends and lessons learned. *Infect. Dis. Clin. North Am.* **30**, 377–390 (2016). <https://doi.org/10.1016/j.idc.2016.02.004>
2. S. Shaikh, N. Nazam, S.M.D. Rizvi, K. Ahmad, M.H. Baig, E.J. Lee, I. Choi, Mechanistic insights into the antimicrobial actions of metallic nanoparticles and their implications for multidrug resistance. *Int. J. Mol. Sci.* (2019). <https://doi.org/10.3390/ijms20102468>
3. O. Lushchak, A. Zayachkivska, A. Vaiserman, Metallic nanoantioxidants as potential therapeutics for type 2 diabetes a hypothetical background and translational perspectives. *Oxid. Med. Cell Longev.* (2018). <https://doi.org/10.1155/2018/3407375>
4. L. Wang, C. Hu, L. Shao, The antimicrobial activity of nanoparticles present situation and prospects for the future. *Int. J. Nanomed.* **12**, 227–249 (2017). <https://doi.org/10.2147/IJN.S121956>
5. T.C. Dakal, A. Kumar, R.S. Majumdar, V. Yadav, Mechanistic basis of antimicrobial actions of silver nanoparticles. *Front Microbiol.* (2016). <https://doi.org/10.3389/fmicb.2016.01831>
6. R. Behra, L. Sigg, M.J.D. Clift, F. Herzog, M. Minghetti, B. Johnston, A. Petri-Fink, B. Rothen-Rutishauser, Bioavailability of silver nanoparticles and ions from a chemical and biochemical perspective. *J. R. Soc. Interface.* **10**, 20130396 (2013). <https://doi.org/10.1098/rsif.2013.0396>
7. I.-M. Chung, I. Park, K. Seung-Hyun, M. Thiruvengadam, G. Rajakumar, Plant-Mediated synthesis of silver nanoparticles their characteristic properties and therapeutic applications. *Nanoscale Res. Lett.* **11**, 40 (2016). <https://doi.org/10.1186/s11671-016-1257-4>
8. S. Ahmed, M. Ahmad, B.L. Swami, S. Ikram, A review on plants extract mediated synthesis of silver nanoparticles for antimicrobial applications a green expertise. *J. Adv. Res.* **7**, 17–28 (2016). <https://doi.org/10.1016/j.jare.2015.02.007>
9. A. Martínez-Abad, Multifunctional and nanoreinforced polymers for food packaging, (Elsevier, New York (2011)). <https://doi.org/10.1533/9780857092786.3.347>
10. S.-L. Abram, J. Gagnon, M. Priebe, N. Héroult, K.M. Fromm, Ag nanoencapsulation for antimicrobial applications. *Chimia (Aarau)*. **72**, 49–252 (2018). <https://doi.org/10.2533/chimia.2018.249>
11. M. Priebe, J. Widmer, N. Suhartha Löwa, S.L. Abram, I. Mottas, A.K. Woischnig, P.S. Brunetto, N. Khanna, C. Bourquin, K.M. Fromm, Antimicrobial silver-filled silica nanorattles with low immunotoxicity in dendritic cells, *Nanomed. Nanotechnol. Biol. Med.* **13**, 11–22 (2017). <https://doi.org/10.1016/j.nano.2016.08.002>
12. Q.B. Xu, L.J. Xie, H. Diao, F. Li, Y.Y. Zhang, F.Y. Fu, X.D. Liu, Antibacterial cotton fabric with enhanced durability prepared using silver nanoparticles and carboxymethyl chitosan. *Carbohydr Polym.* **177**, 187–193 (2017). <https://doi.org/10.1016/j.carbpol.2017.08.129>
13. T.I. Shaheen, A.A.A. El Aty, In-situ green myco-synthesis of silver nanoparticles onto cotton fabrics for broad spectrum antimicrobial activity. *Int. J. Biol. Macromol.* **118**, 2121–2130 (2018). <https://doi.org/10.1016/j.ijbiomac.2018.07.062>
14. S. Kaul, N. Gulati, D. Verma, S. Mukherjee, U. Nagaich, Role of nanotechnology in cosmeceuticals a review of recent. *Adv. J. Pharm.* **2018**, 1–19 (2018). <https://doi.org/10.1155/2018/3420204>
15. E.O. Sousa, J.G.M. Costa, Genus lantana Chemical aspects and biological activities. *Brazilian J Pharmacogn.* **22**, 1155–1180 (2012). <https://doi.org/10.1590/S0102-695X2012005000058>
16. S.S. Azam, A. Habib, A.S. Memic, M. Ahmed, M. Oves, M.S. Khan, Antimicrobial activity of metal oxide nanoparticles against Gram-positive and Gram-negative bacteria a comparative study. *Int. J. Nanomed.* **7**, 6003–6009 (2012). <https://doi.org/10.2147/IJN.S35347>
17. M.I. Masum, M.M. Siddiq, K.A. Ali, Y. Zhang, Y. Abdallah, E. Ibrahim, W. Qiu, C. Yan, B. Li, Biogenic synthesis of silver nanoparticles using phyllanthus emblicafuit extract and its inhibitory action against the pathogen acidovorax oryzaestrain RS-2 of rice bacterial brown stripe. *Front Microbiol.* (2019). <https://doi.org/10.3389/fmicb.2019.00820>

18. C. Ponce, J. Chanona, V. Garibay, E. Palacios, G. Calderon, R. Sabo, Functionalization of agave cellulose nanoparticles and its characterization by microscopy and spectroscopy techniques, *microsc microanal.* **19**, 200–201 (2013). <https://doi.org/10.1017/S1431927613002997>.
19. E.S. Madivoli, E.G. Maina, P.K. Kairigo, M.K. Murigi, J.K. Ogilo, J.O. Nyangau, P.K. Kimani, C. Kipyegon, In vitro antioxidant and antimicrobial activity of *Prunus africana* (Hook. f.) Kalkman (bark extracts) and *Harrisonia abyssinica* Oliv. extracts (bark extracts) a comparative study, *J. Med. Plants Econ. Dev.* (2018). <https://doi.org/10.4102/jomped.v2i1.39>.
20. L. Katata-Seru, T. Moremedi, O.S. Aremu, I. Bahadur, Green synthesis of iron nanoparticles using *Moringa oleifera* extracts and their applications removal of nitrate from water and antibacterial activity against *Escherichia coli*. *J. Mol. Liq.* **256**, 296–304 (2018). <https://doi.org/10.1016/j.molliq.2017.11.093>
21. D. Ciolacu, F. Ciolacu, P.V. Popa, Amorphous cellulose—structure and characterization, *Cellul. Chem. Technol.* **45**, 3–21
22. Z. Wang, C. Fang, M. Megharaj, Characterization of iron-polyphenol nanoparticles synthesized by three plant extracts and their fenton oxidation of azo dye. *ACS Sustain. Chem. Eng.* **2**(2014), 1022–1025 (2018). <https://doi.org/10.1021/sc500021n>
23. Y.Y. Loo, Y. Rukayadi, M.-A.-R. Nor-Khaizura, C.H. Kuan, B.W. Chieng, M. Nishibuchi, S. Radu, In vitro antimicrobial activity of green synthesized silver nanoparticles against selected gram-negative foodborne pathogens. *Front Microbiol.* **9**, 1555 (2018). <https://doi.org/10.3389/fmicb.2018.01555>
24. J. Olson, S. Dominguez-Medina, A. Hoggard, L.Y. Wang, W.S. Chang, S. Link, Optical characterization of single plasmonic nanoparticles. *Chem. Soc. Rev.* **44**, 40–57 (2015). <https://doi.org/10.1039/c4cs00131a>
25. S.I. Vasylevskyi, S. Kracht, P. Corcosa, K.M. Fromm, B. Giese, M. Füeg, Formation of silver nanoparticles by electron transfer in peptides and c-cytochromes. *Angew. Chem. Int. Ed.* **56**, 5926–5930 (2017). <https://doi.org/10.1002/anie.201702621>
26. M. Ndikau, N.M. Noah, D.M. Andala, E. Masika, Green synthesis and characterization of silver nanoparticles using *Citrullus lanatus* fruit rind extract. *Int. J. Anal. Chem.* (2017). <https://doi.org/10.1155/2017/8108504>
27. X.C. Jiang, W.M. Chen, C.Y. Chen, S.X. Xiong, A.B. Yu, Role of temperature in the growth of silver nanoparticles through a synergetic reduction approach. *Nanoscale Res. Lett.* **6**, 1–9 (2011). <https://doi.org/10.1007/s11671-010-9780-1>
28. N. Ahmad, B.C. Ang, M.A. Amalina, C.W. Bong, Influence of precursor concentration and temperature on the formation of nanosilver in chemical reduction method, *Sains Malaysiana.* **47**, 57–168 (2018). <https://doi.org/10.17576/jsm-2018-4701-19>.
29. M. Vanaja, K. Paulkumar, M. Baburaja, S. Rajeshkumar, G. Gnanajobitha, C. Malarkodi, M. Sivakavinesan, G. Annadurai, Degradation of methylene blue using biologically synthesized silver nanoparticles. *Bioinorg. Chem. Appl.* (2014). <https://doi.org/10.1155/2014/742346>
30. G. Socrates, *Infrared and Raman Characteristic Group Frequencies*, 3rd edition, 2001. <https://doi.org/10.1002/jrs.1238>.
31. C. Levard, S. Mitra, T. Yang, A.D. Jew, A.R. Badireddy, G. V. Lowry, G.E. Brown, Effect of chloride on the dissolution rate of silver nanoparticles and toxicity to *E. coli*, *Environ. Sci. Technol.* **47**, 5738–5745 (2013). <https://doi.org/10.1021/es400396f>.
32. J. Hoyos-Arbeláez, M. Vázquez, J. Contreras-Calderón, Electrochemical methods as a tool for determining the antioxidant capacity of food and beverages a review. *Food Chem.* **221**, 1371–1381 (2017). <https://doi.org/10.1016/j.foodchem.2016.11.017>
33. M. José Jara-Palacios, M. Luisa Escudero-Gilete, J. Miguel Hernández-Hierro, F.J. Heredia, D. Hernanz, Cyclic voltammetry to evaluate the antioxidant potential in winemaking by-products, *Talanta.* **165**, 211–215 (2017). <https://doi.org/10.1016/j.talanta.2016.12.058>.
34. L.C. Yun'an Qing, R. Li, G. Liu, Y. Zhang, X. Tang, J. Wang, H. Liu, Y. Qin, Potential antibacterial mechanism of silver nanoparticles and the optimization of orthopedic implants by advanced modification technologies, *Int. J. Nanomed.* **13**, 3311–3327 (2018). <https://doi.org/10.2147/IJN.S165125>.

Publisher's Note Springer Nature remains neutral with regard to jurisdictional claims in published maps and institutional affiliations.